The Topological Entropy for an Inclined Billiard in a Gravitational Field *

Jürgen Vollmer

Institut für Physik, Universität Basel, Klingelbergstrasse 82, CH-4056 Basel, Switzerland

Z. Naturforsch. **49a**, 861–870 (1994); received May 30, 1994

A new parameterization for an inclined billiard initially discussed by Hénon is presented. This parameterization expresses the time evolution of the scattering system by a family of pruned baker transformations. This allows to make contact with recent work on these mappings. As an application, the topological entropy is analytically derived in a very good approximation and it is indicated how to systematically improve the result. The result which contains no free parameter, agrees excellently with numerical data for the whole parameter range from strongly chaotic scattering described by a complete symbolic dynamics to a bounded system with trivial scattering behavior.

05.45.+b, 03.20.+i, 05.90.+m

I. Introduction

Recently Hénon introduced an inclined billiard in a gravitational field [1] that serves as a model for chaotic scattering, and pointed out that in a certain parameter range the system is described by a piecewise linear map. He worked out a symbolic dynamics description of the invariant set of the map and discussed how the scattering behavior is related to the symbol sequences. Analytical results were obtained for the parameter range where the symbolic dynamics is complete, and some numerical data were presented for other parameter values. In this paper an alternative representation for the model is presented that allows to make contact with the present author's work on transient chaos [2, 3] in a class of pruned baker transformations. This is interesting in itself, as it places Hénons results in a wider context. Besides being relevant for chaotic scattering, as e.g. in satellite encounters [4], Hénon's results are connected to aspects of spatial chaos in Frenkel-Kontorova-like systems [2, 5, 6], to the storage capacity of an optical memory under unfavorable working conditions [7], and to transient chaos in dissipative, Lorenz-like maps [8–10].

Moreover, results on the symbolic dynamics for the pruned baker transformations allow to discuss the properties of the inclined billiard in a parameter range not treated be Henon: In the following it is pointed out that both, the occurrence of forbidden sequences in the symbolic dynamics and the disappearing of transient orbits close to the transition of the scattering system to a closed system are due to escaping orbits. This is in close analogy to the situation at crises in dissipative [11] and in chaotic scattering [12] systems. The arguments allow to calculate the topological entropy of the scattering problem to a very good approximation for *all* parameter values where the description by piecewise linear maps in possible.

In the following we first revisit Hénon's description of the inclined billiard (Section II). Subsequently we derive scaling laws describing the topological entropy at the onset of scattering (Section III A) and at the occurrence of forbidden sequences (Section III B). In Section III C these results are compared to numerical data, and possibilities are discussed on how to systematically derive corrections to the scaling laws. The paper concludes with a summary and discussion (Section IV).

II. The Inclined Billiard Revisited

A) Derivation of the Map

Consider a point particle moving in the (X, Y)-plane. It is elastically reflected at two fixed circular disks with centers $(-a, -r)$ and $(+a, -r)$ and radius r (Figure 1). In addition, due to a gravitational field the particle feels a constant acceleration g in the negative Y-direction.

At a fixed energy the trajectory of a particle is uniquely characterized by the sequence of X-co-

* Paper presented at the 4th Annual Meeting of ENGADYN, Grenoble, October 11–14, 1993.

Reprint requests to Dr. J. Vollmer, Institut für Physik, Universität Basel, Klingelbergstrasse 82, CH-4056 Basel/Schweiz

0932-0784 / 94 / 0900-0861 $ 06.00 © – Verlag der Zeitschrift für Naturforschung, D-72027 Tübingen

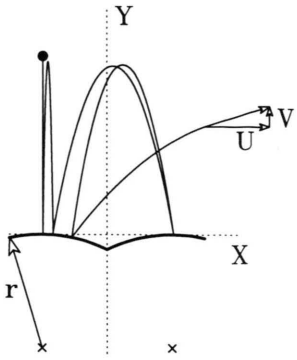

Fig. 1. Typical trajectory of a particle bouncing from two circular disks and the relevant parameters to describe its movement. The centers of the disks are given by the crosses in the plot. They lie at $(X, Y) = (-a, -r)$ and $(X, Y) = (+a, -r)$. U and V denote the velocity of the particle in horizontal and vertical direction, respectively.

ordinates at successive reflections: $\langle X_{n+i}\rangle_i \equiv \langle \ldots X_{n-2}X_{n-1} \cdot X_n X_{n+1} \ldots\rangle$. This sequence may be viewed as a time series describing the evolution of the system. For the description of the motion within the scattering region, the X_i may be restricted to the interval $X_i \in [-1, +1]$ [13] because the particle escapes to $+\infty\,(-\infty)$ after passing the right (left) hill. In this notation of the time series, the dot represents system time. It indicates that the particle is on its way from X_{n-1} to X_n.

The billiard has two degrees of freedom. On account of energy conservation two successive X-coordinates uniquely specify the time evolution of the system. They may be viewed as delay coordinates for an embedding of the invariant set of the chaotic scattering system [13, 14]. For $rE \gg mga^2$ the corresponding mapping is well approximated by the linear map (cf. Appendix A)

$$\begin{pmatrix} X_{n+1} \\ X_n \end{pmatrix} = \begin{pmatrix} 2\gamma & -1 \\ 1 & 0 \end{pmatrix} \begin{pmatrix} X_n \\ X_{n-1} \end{pmatrix} + \sigma_n \begin{pmatrix} 2\gamma - 2 \\ 0 \end{pmatrix}, \tag{1}$$

where

$$\gamma = 1 + 4E/mgr, \tag{2}$$

$$\sigma_n = \operatorname{sign}(X_n). \tag{3}$$

The map has eigenvalues

$$\eta^{\pm 1} = \gamma \mp (\gamma^2 - 1)^{1/2} \tag{4}$$

and eigendirections $(1, \eta)$ and $(1, \eta^{-1})$, where $0 \leq \eta \leq 1$. η is small for large E/mgr and it approaches 1 for $E/mgr \to 0^+$.

For $\eta \neq 1$ the map (1) may be diagonalized by an affine linear transformation, which yields

$$\mathscr{F}: \begin{pmatrix} x \\ y \end{pmatrix} \to \begin{pmatrix} \eta & 0 \\ 0 & \eta^{-1} \end{pmatrix} \begin{pmatrix} x \\ y \end{pmatrix} + \sigma_n \begin{pmatrix} 1-\eta \\ 1-\eta^{-1} \end{pmatrix}. \tag{5}$$

This is a piecewise linear map with fixed points $(-1, -1)$ and $(+1, +1)$. The branches of $\mathscr{F}$ are set by the conditions $\sigma_n = +1$ and $\sigma_n = -1$, respectively. They are separated by an inclined line $\mathscr{L}$ (the *critical line*) with slope $-\eta$,

$$\mathscr{L}: \; y = -\eta x. \tag{6}$$

This is a pruned baker transformation. In contrast, Hénon starts from a Poincaré section with X_n and the horizontal velocity of the outgoing particle immediately after reflection (denoted by U_n in Appendix A) as free parameters, and diagonalizes that map [1, 15]. The advantages of the parameterization (5) of the scattering system lies in the fact that it allows to make contact with results on pruned baker transformations.

B) Structure of the Invariant Set

One easily verifies that the invariant set of $\mathscr{F}$ is contained in the square $\mathscr{U}$: $[-1, +1] \times [-1, +1]$. The application of $\mathscr{F}$ on $\mathscr{U}$ is illustrated in Figure 2: First U is squeezed in x-direction by a factor η and stretched in y-direction by a factor η^{-1} (*stretching*). Then the resulting rectangle is cut along the line $\mathscr{F}(\mathscr{L})$: $y = \eta^{-1} x$, and the upper part is shifted back to the right-hand edge of the square $\mathscr{U}$ (*folding*). To stress the symmetry of the map, $\mathscr{U}$ may be cut along $\mathscr{L}$ first and then stretched on the two half-planes separately (Figure 3). We will use this representation in the following. Because the scattering problem is invariant under reflection of X-coordinates ($X \rightleftharpoons -X$) the critical line has to go through the origin of the (x, y)-plane. The demand for bijectivity on the whole plane fixes the slope of $\mathscr{L}$ to $-\eta$. The nonzero slope of $\mathscr{L}$ is the essential difference with respect to baker transformations studied elsewhere (e.g. in [17]), as

- it allows to interpret $\mathscr{F}$ as a bijective mapping on the whole plane, and
- it is responsible for the occurrence of missing sequences in the appropriate symbolic dynamics (see below).

For $\eta < 0.5$ the image of $\mathscr{U}$ consists of two vertical trapezoids of width η, and the pre-image lies in hori-

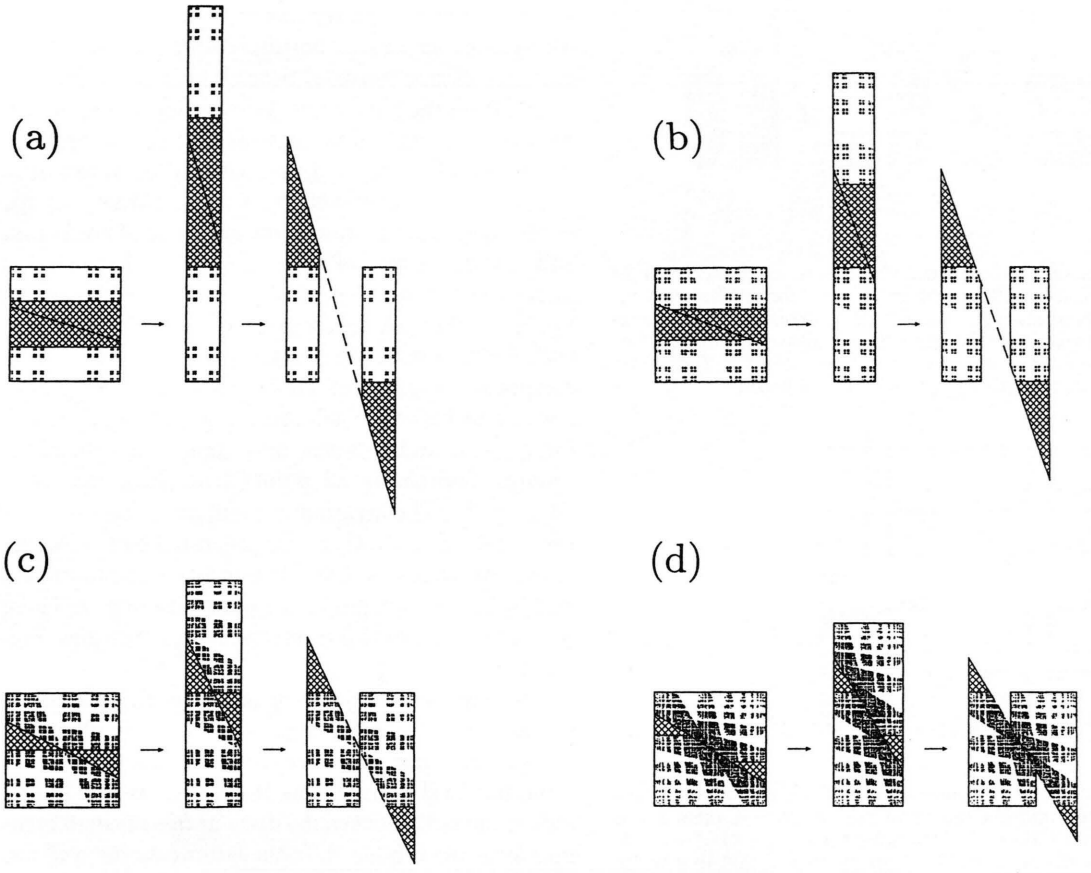

Fig. 2. Stretching and folding for the pruned baker transformation as given by (5). Details on how to label the axis are given in Fig. 4 below. – (a) $\eta = 0.3$: There is a horizontal band leaving $\mathcal{U}$ in one iteration (double hatched area) and vertical band with no pre-images in $\mathcal{U}$. The invariant set is a complete Cantor set. It is obtained by taking away all pre-images of the horizontal band, and all images of the vertical band. – (b) $\eta = \frac{\sqrt{3}-1}{2} \approx 0.366$: Two additional triangles have emerged that leave the invariant set. The occurrence of pruning is due to trajectories of the former invariant set that enter these *escape triangles*. – (c) $\eta = 0.5$: This is a borderline case. The width of the horizontal band has shrunk to zero. As a consequence there is no a priori Cantor set due to the bands any longer that supports the invariant set. The fractal structure of the invariant set is only due to taking away the images and pre-images of the escape triangles (double hatched area). – (d) $\eta = \frac{\sqrt{5}-1}{2}$ ≈ 0.618: There are two escape triangles (double hatched areas) with points that leave the invariant set under one application of $\mathcal{F}$ and two with no pre-images in $\mathcal{U}$. (The data points in this figure show a numerical approximation to the chaotic saddle. They were initially published in [16].)

zontal trapezoids of the same width (Figs. 2 a, b and 3). Thus an argument analogous to the one used in the construction of a Smale horseshoe [17] shows that the invariant set of $\mathcal{F}$ is contained in a two-dimensional Cantor set with scaling η in both directions. The half-planes above and below the critical line $\mathcal{L}$ form a generating partition for a symbolic dynamics description of the invariant set. Points (x_n, y_n) of the invariant set uniquely correspond to symbol sequences $<\sigma_{n+i}>_{i=-\infty}^{+\infty}$, where σ_{n+i} takes the value -1 $(+1)$ when $\mathcal{F}^i(x_n, y_n)$ lies below (above) the critical line [10]. All points that share the same finite symbol subsequence (*word*) $\langle\sigma_{n+i}\rangle_{i=-k}^{k-1}$ lie in a square of size $2^{-k} \times 2^{-k}$ (a *k-box*) that is contained in $\mathcal{U}$. The k-boxes give a refining partition of the invariant set. They contain points that do no leave $\mathcal{U}$ under $(k-1)$-fold forward backward iteration. The 1- and 2-boxes are shown in Figure 4.

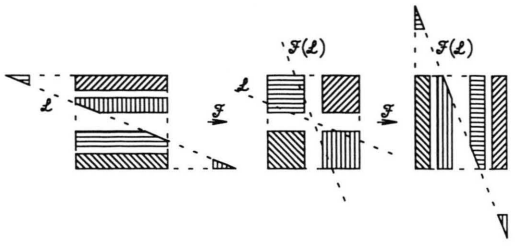

Fig. 3. Generalized baker transformation as given by (5). In order to visualize the action of $\mathscr{F}$ the 1-boxes (hatched regions in the middle part) and their images and pre-images under $\mathscr{F}$ are drawn. The parts below (above) the critical line $\mathscr{L}$ are mapped by the upper (lower) branch of $\mathscr{F}$. Details on how to label the axis are given in Fig. 4 below.

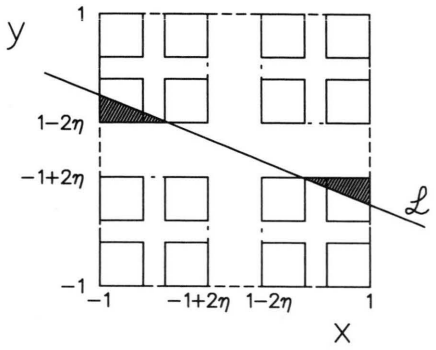

Fig. 4. First level (short dashes) and second level (solid line) boxes approximating the invariant set. The Cantor set is contained in $\mathscr{U}$ (long dashes), which is $[-1,+1]\times[-1,+1]$ for our definition of $\mathscr{F}$. The 1-boxes have height and width η. The intersection of the critical line $\mathscr{L}$ with the 1-boxes gives rise to escape regions (hatched triangles).

Points outside the Cantor set always correspond to transient orbits. They proceed to $y=\pm\infty$ under repeated iteration with $\mathscr{F}$ and $\mathscr{F}^{-1}$, respectively. In contrast, all points of the Cantor set represent bounded trajectories as long as the critical line does not intersect the 1-boxes, i.e. for $\eta<\frac{1}{3}$. In that case the symbolic dynamics is complete. For the scattering system this implies that there are scattering trajectories that scatter in any desired sequence at the two disks, provided that $E\geq\frac{1}{6}mgr$.

For $\eta>\frac{1}{3}$ the critical line intersects the 1-boxes. The triangle formed by the lower left corner of the upper left 1-box and $\mathscr{L}$ is referred to as an *escape triangle* in the following, as points of the Cantor set that enter this region escape to $y=\infty$ under forward iteration. Another escape triangle is formed by the upper right corner of the lower right 1-box and $\mathscr{L}$. Points entering this region escape to $y=-\infty$ (Figs. 2b and 4). Analogously, the triangles formed by $\mathscr{F}(\mathscr{L})$ and the 1-boxes form escape regions for backward iteration. All symbol sequences corresponding to points that enter the escape triangles become forbidden, they are *pruned* from the binary tree representing all sequences. As a consequence some sequences of scattering from the two disks are no longer realized by the trajectories.

The Cantor set-structure of the invariant set for $\eta<0.5$ (Fig. 2a, b) is due to the existence of horizontal and vertical stripes of width $2(1-2\eta)$ that leave $\mathscr{U}$ under one application of $\mathscr{F}$ and $\mathscr{F}^{-1}$, respectively. For $\eta<\frac{1}{3}$ they are the complements of $\mathscr{F}^{-1}(\mathscr{U})\cap\mathscr{U}$ and $\mathscr{F}(\mathscr{U})\cap\mathscr{U}$, respectively. At $\eta>0.5$ these stripes disappear (Figure 2c). Nevertheless, the half-planes above and below $\mathscr{L}$ still form a generating partition for $\eta\geq0.5$, and k-boxes may again be defined as squares, containing all points that share the word $\langle\sigma_{n+i}\rangle_{i=-k}^{k-1}$. The invariant set still has a fractal structure for $0.5\leq\eta<1$: Gaps are generated by the images of the two triangles inside $\mathscr{U}$ that have no pre-images and by the pre-images of the points leaving $\mathscr{U}$. These points again lie in two respective *escape triangles* (Figure 2d).

The gaps vanish when η tends to 1. This corresponds to the limit $E/mgr\to0$. At $\eta=1$ either the energy of the particle is zero or the radius of the disks is infinite. In the former case the particle can no longer escape the well between the disks and the system turns into a bounded billiard. In the latter case the well has disappeared. To obtain the linear map (1) we restricted the discussion to $rE\gg mga^2$. In that case $r\to\infty$ and the points on the diagonal $X_n=X_{n+1}$ form the invariant set of (1). All these points are fixed points. Initial conditions away from the diagonal correspond to particles that move with constant velocity. Note that the eigendirections of (1) are parallel for $\eta=1$. Therefore the affine linear transformation from (1) to (5) becomes singular: $\mathscr{F}$ is the identical map on the whole plane. It still describes the fixed points on the diagonal of the (X_n, X_{n+1})-plane, but the time evolution of all other points is lost by the transformation. Moreover, the half-planes above and below $\mathscr{L}$ do no longer form a generating partition as all fixed points in each half-plane share the same symbol sequence: The encoding is no longer unique.

III. Parameter Dependence of the Topological Entropy

The topological entropy K_0 measures the asymptotic exponential growth of the number $M_{2k}(\eta)$ of

allowed words $\langle \sigma_{n+i} \rangle_{i=-k}^{k-1}$ with their length $2k$:

$$M_{2k}(\eta) \propto \exp(K_0 2k) \quad \text{for large } k. \tag{7}$$

It is a measure for the complexity of the time evolution of a dynamical system [17, 18]. The topological entropy of the invariant set of $\mathscr{F}$ takes its maximum value log 2 when all symbol sequences are allowed, i.e. for $\eta < \frac{1}{3}$. For larger η the topological entropy K_0 decreases and it approaches 0 when η tends towards 1 [2]. In the following, statistical arguments are used to calculate $K_0(\eta)$ in the parameter range $0 \leq \eta < 1$.

Prior to this discussion the author would like to point out that one can use the following arguments to discuss the fractal dimension D or the escape rate $\varkappa$ of the invariant set as well. For piecewise linear maps the Lyapunov exponents ($\pm \log \eta^{-1}$ in the case of $\mathscr{F}$) are constant for all trajectories, and the latter quantities may immediately be calculated from K_0 due to the relations

$$D_0 = K_0 / \log \eta, \tag{8a}$$

$$\varkappa = -K_0 - \log \eta, \tag{8b}$$

which follow from the thermodynamic formalism [19]. The topological entropy has been chosen as it only changes when there are bifurcations, i.e. when new forbidden words occur, and it is constant otherwise. In contrast, $\varkappa$ and D_0 vary in the whole parameter range and it is more difficult to keep apart the additional contributions due to bifurcations.

A) Scaling Behavior at the Onset of Chaotic Scattering

There is no scattering for $\eta = 1$. In particular, there is no chaotic behavior and therefore K_0 is zero [20]. At this parameter value every point is a fixed point. For smaller η the invariant set of $\mathscr{F}$ is contained in $\mathscr{U}$. There are small escape regions in $\mathscr{U}$ and points entering these regions are mapped to infinity under repeated application of $\mathscr{F}$ (Figure 2d). This situation is reminiscent of a boundary crisis in strange attractors of dissipative systems [11]. In fact, the arguments proposed for the calculation of the escape rate $\varkappa$ at a crisis apply also in our case. They only need to be generalized from a parabolic to a triangular form of the escape region [19]. A careful analysis of the geometry of the invariant set allows to explicitly calculate $\varkappa$ and not only the exponent of its power-law dependence. K_0 may be calculated from $\varkappa$ by (8b) which follows from the thermodynamic formalism.

The escape rate $\varkappa$ measures how quickly trajectories are expelled from a neighborhood of the invariant set. This rate may be calculated by uniformly distributing a large number N_0 of initial points in $\mathscr{U}$ and monitoring how many trajectories N_n that started out at the initial points are still staying in $\mathscr{U}$ after n iterations.

$$N_n \propto N_0 \exp(-\varkappa n), \quad \text{for large } n. \tag{9}$$

The escape rate is zero when the system is closed (in our case for $\eta = 1$) and it is finite for a (chaotic) scattering system (i.e. for $0 \leq \eta < 1$ in the case of $\mathscr{F}$).

The escape rate may be calculated by a statistical argument: A trajectory leaves $\mathscr{U}$ if and only if it enters one of the two escape triangles that leave the square in the next step of iteration (cf. Figure 2d). $\mathscr{F}$ has a constant natural measure because it is a piecewise linear map. Hence, the probability to leave $\mathscr{U}$ in one step is proportional to the relative size $\mathscr{P}$ of the escape triangles with respect to the area $A = 4$ of $\mathscr{U}$:

$$\mathscr{P} = \frac{1}{4} \Delta x \, \Delta y = \frac{1}{4\eta} (1-\eta)^2, \tag{10}$$

where $\Delta y = \eta - (-1 + 2\eta) = 1 - \eta$ and $\Delta x = \Delta y / \eta$ denotes the width and the height of the escape triangles, respectively.

Dynamical systems such as the pruned baker transformations studied in this paper typically show ergodicity and mixing properties on the invariant set [21]. As a consequence correlations between the probabilities to enter the triangles in successive steps decay exponentially fast. Therefore the number N_n of points remaining in $\mathscr{U}$ after n iterations is well approximated by

$$N_n = N_0 (1 - \mathscr{P})^n, \tag{11}$$

which yields the escape rate

$$\varkappa = -\log(1 - \mathscr{P}) \approx \frac{1}{4\eta} (1-\eta)^2. \tag{12}$$

For $\eta \lesssim 1$ this is the well-known scaling behavior for $\varkappa$ [11]. However, in the present case it is also possible to calculate the pre-factor of the scaling law and its logarithmic corrections. The formula may be used as long as the invariant set is not embedded in a Cantor set, i.e. for $0.5 \leq \eta < 1$. For smaller values of η, the gaps of the Cantor set give additional contributions to the escape that are not accounted for in the above argument.

For $\mathscr{F}$ the Lyapunov exponent, the escape rate and the topological entropy are related by (8b), so that one

obtains

$$K_0(\eta) = -\log\eta - \log\left(1 - \frac{1}{4\eta}(1-\eta)^2\right) \approx (1-\eta) + \frac{2\eta+1}{4\eta}(1-\eta)^2, \quad \text{for } 0.5 \leq \eta < 1. \tag{13}$$

The terms in $(1-\eta)$ are the two leading orders of an expansion of K_0 for $\eta \lesssim 1$. The leading term may be deduced from the observation that the fractal dimension of the invariant set is 2 when there is no escape. The quadratic term contains corrections due to escape. As far as the author sees, correlations that are dropped by the statistical argument only change higher-order terms in the expansion. Their contributions may be systematically calculated by expanding the symbolic dynamics into Markov chains [18].

B) Scaling Behavior at the Onset of Pruning

For $0 < \eta < \frac{1}{3}$ the invariant set of $\mathscr{F}$ is a full two-dimensional Cantor set with a symbolic dynamics as known from the baker transformation. Any binary symbol sequence uniquely corresponds to a point of the invariant set. For this parameter range the scattering system described by $\mathscr{F}$ has been treated in detail by Hénon [1].

For $\eta = \frac{1}{3}$ the homoclinic orbit corresponding to the symbol sequence $\langle(-1)^\infty(+1)(-1)^\infty\rangle$ touches the critical line a that point which is located at the lower left corner of the upper left 1-box. At this parameter value the trajectory splits into two transients that approach the fixed point $(x, y) = (-1, -1)$ under backward (forward) iteration and escape $\mathscr{U}$ under forward (backward) iteration. The points of these transients still lie in the Cantor set. However, they are no longer part of the invariant set of $\mathscr{F}$, and the corresponding symbol sequences become forbidden (pruned). By symmetry reasons the homoclinic orbit with the symbol sequence $\langle(+1)^\infty(-1)(+1)^\infty\rangle$ becomes forbidden at the same parameter value.

For $\eta > \frac{1}{3}$ most of the trajectories escape. Geometrically they may be characterized by the condition that they contain a point that enters one of the escape triangles given by the intersection of $\mathscr{L}$ with the upper left and lower right 1-box, respectively (Figs. 3 and 4). All corresponding symbol sequences become forbidden and K_0 starts to decrease. In order to calculate K_0, one needs to know the number of forbidden words. A word of length $2k$ may uniquely be identified with one of 2^{2k} k-boxes. All trajectories passing through this box contain the word in their symbol sequences. The word is forbidden if any of the trajectories starting in the box enter an escape triangle under at most $(k-1)$ forward or k backward iterations, because by definition all points of a box stay at the same side of $\mathscr{L}$ during these iterations.

After this consideration the deviation of K_0 from its maximum value may again be calculated by a statistical argument: Denoting the fraction of k-boxes in the escape triangles by $\mathscr{P}$ and neglecting correlation as above one finds the topological entropy,

$$\begin{aligned} K_0(\eta) &= \lim_{k\to\infty} \frac{1}{2k} \log\left((1-\mathscr{P})^{2k} 2^{2k}\right) \\ &= \log 2 + \log(1-\mathscr{P}) \\ &\approx \log 2 - \mathscr{P}, \quad \text{for small } \mathscr{P}. \end{aligned} \tag{14}$$

The probability $\mathscr{P}$ denotes the fraction of boxes in two escape triangles of width Δx and height Δy (Figure 4). Since the boxes form a refining partition of the Cantor set, the number of k-boxes in the triangles scales with the partial fractal dimensions D_x and D_y of the Cantor set supporting the invariant set:

$$\mathscr{P} \propto (\Delta x)^{D_x} (\Delta y)^{D_y}. \tag{15}$$

From the construction of the Cantor set one easily verifies that $D_x = D_y = -\dfrac{\log 2}{\log \eta}$. The height and width of the escape triangles $\Delta y = \dfrac{1+\eta}{2} - (1-\eta) = \dfrac{3\eta-1}{2}$ and $\Delta x = \dfrac{\Delta y}{\eta}$ immediately follow from the geometry of the 1-boxes and the equation for $\mathscr{L}$ (Figure 4). The pre-factor in (15) is fixed by normalizing Δx and Δy with respect to the side length of $\mathscr{U}$. Inserting (15) into (14) one obtains

$$\begin{aligned} K_0(\eta) &= \log 2 + \log\left(1 - \left(\frac{9}{4\eta}\right)^{D_x}\left(\eta - \frac{1}{3}\right)^{2D_x}\right) \\ &\approx \log 2 - \left(\frac{9}{4\eta}\right)^{D_x}\left(\eta - \frac{1}{3}\right)^{2D_x}, \\ &\qquad \text{for } \frac{1}{3} \leq \eta \leq \frac{1}{2}. \end{aligned} \tag{16}$$

The result is valid for $\frac{1}{3} \leq \eta \leq \frac{1}{2}$. For smaller η there is no pruning and for $\eta > \frac{1}{2}$ the underlying Cantor set-structure disappears.

C) Numerical Test and Extensions of the Result

As discussed in the two previous subsections, we have used statistical arguments and a relation between K_0, $\varkappa$, and η following from the thermodynamic formalism to describe the behavior of K_0 in the whole range $0 \leq \eta < 1$ (solid line in Fig. 5a):

$$K_0(\eta) = \begin{cases} \log 2, & \text{for } 0 \leq \eta \leq \frac{1}{3}, \\ \log 2 + \log\left(1 - \left(\frac{9}{4\eta}\right)^{D_\varkappa}\left(\eta - \frac{1}{3}\right)^{D_\varkappa + D_\varkappa}\right) & \text{for } \frac{1}{3} \leq \eta \leq \frac{1}{2}, \\ -\log\eta - \log\left(1 - \frac{1}{4\eta}(1-\eta)^2\right) & \text{for } \frac{1}{2} \leq \eta < 1, \\ 0 & \text{for } \eta = 1. \end{cases} \tag{17}$$

Although the results contain no free parameter, they match for the borderline cases $\eta = \frac{1}{3}, \frac{1}{2}$, and 1 where there are two possibilities to calculate K_0. As a consequence $K_0(\eta)$ is continuous in the considered range of η.

To test the quality of the result, we have calculated the topological entropy numerically [2]

- by evaluating the number $M_n(\eta)$ of periodic orbits of length n and using (7),
- by using the thermodynamic formalism [22] to analyze a numerical scattering experiment,
- by a transfer matrix technique.

The numerical methods give consistent results for $0 \leq \eta \lesssim 0.7$. In this parameter range the prediction (17) is in good agreement with the numerical data (Figure 5a).

For $\eta \gtrsim 0.7$ the numerical data are no longer reliable. However, the result (17) is bracketed by exact analytic upper and lower bounds [2] that become tangent in this limit. The upper bound stems from the fact that the fractal dimension of the invariant set of a two-dimensional map cannot exceed two. It corresponds to the first-order term in the expansion (13) in powers of $(1-\eta)$. The lower bound was obtained by explicitly enumerating and counting very stable periodic orbits. Equation (17) is consistent with these bounds. Thus the author is confident that (17) gives a reliable description of K_0 in the whole parameter range $0 \leq \eta \leq 1$.

Due to the approximations made in the derivation there are, of course, deviations between the numerical data and the curve given by (17). They are due to the neglect of correlations when calculating the probability of an orbit to escape. The largest deviation (about 3.5%) is discerned at $\eta = 0.5$. One can easily improve on this. E.g. the error already halves when it is taken into account that the escape regions for forward and backward iteration do not overlap (Figure 5b).

In addition to these deviations from (17), there are oscillating deviations for $\frac{1}{3} < \eta < \frac{1}{2}$. They are easier recognized when the relative error is plotted on a logarithmic scale in $(\eta - \frac{1}{3})$ (lower part of Figure 5c). The oscillations are due to the self-similar structure of the escape triangles. This yields corrections to the relation between the size of the forbidden triangles and the number of boxes they contain. Therefore, there is a fine structure on the *average* behavior (15). An explicit calculation of this fine structure [10] gives an improved parameter-free prediction for K_0 (Figure 5d).

IV. Discussion and Conclusions

In this paper I have discussed the parameter dependence of the topological entropy for an inclined billiard in a gravitational field. It was pointed out that statistical arguments are sufficient to calculate the topological entropy in a good approximation for the whole parameter range from strongly chaotic scattering described by a *complete* binary symbolic dynamics ($\eta < \frac{1}{3}$) to a bounded system with trivial scattering behavior ($\eta = 1$). Hénon showed [1] that any allowed word of the symbolic dynamics corresponds to a set of initial conditions for the scattering system where all trajectories are scattered from the disks in the sequence predetermined by the symbol sequence. The result on K_0 entails that all sequences are allowed for $E \geq \frac{1}{6} mgr$ and that at most a countable number of transient orbits is left for $E/mgr = 0$ In fact, we have argued that there are no transient orbits left at this parameter value, as they either cannot leave the well any longer ($E = 0$) or the well disappeared ($r = \infty$). In addition, it has been shown that the orbits remaining trapped forever are a subset of a regular Cantor set in a time delay map for $E \geq \frac{1}{16} mgr (\eta \leq \frac{1}{2})$. For $E \geq \frac{1}{6} mgr$ ($\eta \leq \frac{1}{3}$) the set is complete, and it vanishes due to the disappearance of gaps in the regular Cantor-set structure. Nevertheless, the invariant set has a fractal structure for all $E/mgr > 0$. For $E < \frac{1}{16} mgr (\eta > \frac{1}{2})$ it is caused by pruning only.

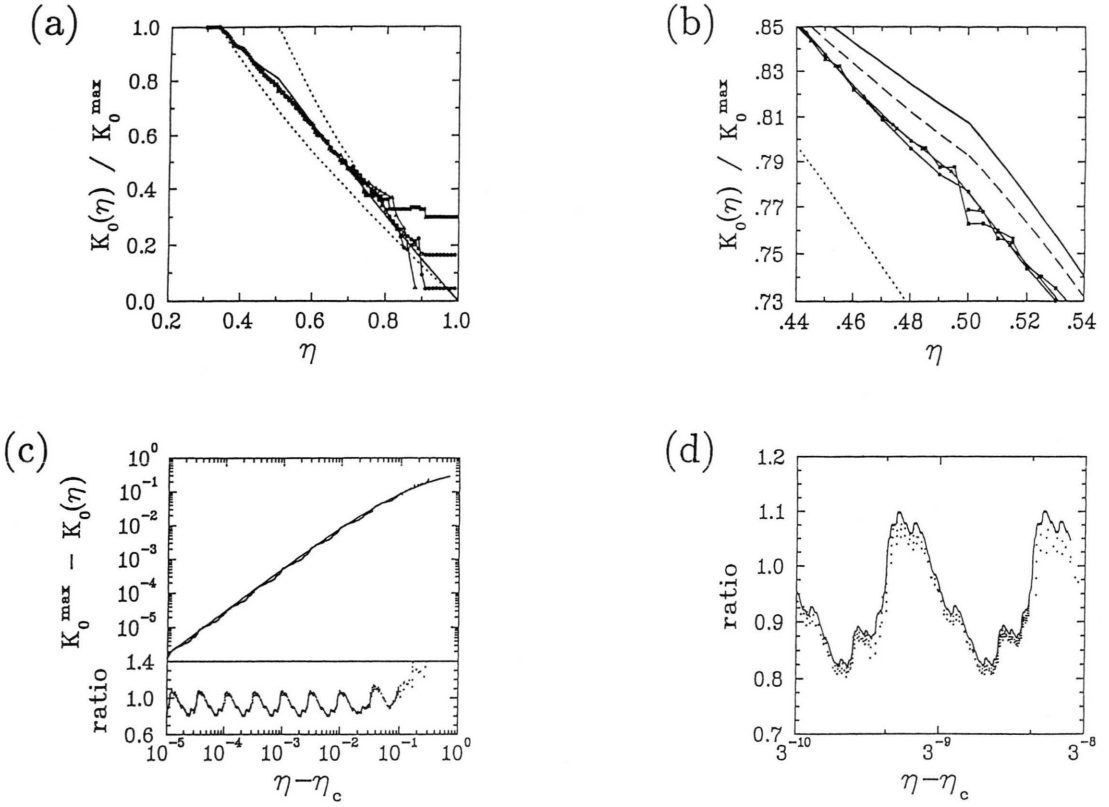

Fig. 5. Numerical test of the results on the topological entropy (17). – (a) Comparison of numerical results obtained by counting periodic orbits, by the scattering formalism and by a transfer matrix method with the theoretical result (17) (solid line). The dotted lines give exact upper and lower bounds on K_0. For details on the numerical methods and on the bounds see [2]. – (b) Close-up of the results for $\eta \approx 0.5$. The inclusion of correlations to first order improves the result (17) considerably (dashed line). – (c) Scaling law at the onset of pruning on a double logarithmic scale (above). The lower part shows the ratio of numerical data and the theoretical result. The periodic oscillations on the logarithmic scale are due to the self-similar fine structure of the Cantor set in the vicinity of the first forbidden orbit. $\eta_c \equiv \frac{1}{3}$ is the parameter value where pruning first occurs. – (d) Comparison between the fine structure of the numerical data and an improved theoretical calculation that accounts for the self-similar fine structure of the Cantor set in the vicinity of the first forbidden orbit.

Although all correlations are neglected in the statistical arguments used for the calculation of K_0, a parameter-free result has been obtained that agrees excellently with numerical data. The accuracy is better than a few percent in the worst case. There is no principal difficulty to improve the accuracy of the approximation by accounting for the self-similar structure of the invariant set and by successively including correlations. The scheme may as well be used to calculate other quantities of interest, e.g. the escape rate and the fractal dimension of the invariant set. As $\mathcal{F}$ is a piecewise linear map the latter quantities are closely related to the topological entropy through the thermodynamic formalism [19]. Therefore the topological entropy is the only nontrivial quantity in this model.

To some extent, the high quality of the theoretical prediction of the topological entropy is due to the simplicity of the map: $\mathcal{F}$ is piecewise linear and does not have multifractal properties. This allows to analytically calculate the pre-factors of the scaling laws at the onset of pruning and at the disappearance of scattering, respectively. In spite of this, the author is confident that the approach presented in this paper is also useful in more complicated systems. After all, similar scaling laws have been studied in the context of crises in attractors of dissipative systems which have turned out to reliably describe experimental [23] and numerical data [11]. Moreover, (14) has successfully been tested for other systems, including pruned baker transformations with multifractal properties [10] and

continuous maps [24]. It is interesting to elaborate on the relation between the crises presented in this paper and crises in dissipative systems: The disappearing of transient chaos may be viewed as the conservative limiting case of a boundary crisis in the attractor of a family of area contracting maps that have been discussed by Tél [9]. The occurring of forbidden orbits is the analogue to a boundary crisis of a dissipative system, in the same sense that the merging crisis in chaotic scattering [12] is related to attractor merging [11].

To summarize, a method has been discussed to determine all topologically different scattering trajectories (the allowed words in the corresponding symbolic dynamics) of an inclined billiard in a gravitational field. This allowed an analytical calculation of the topological entropy. The approach relies on local information in a neighborhood around the first forbidden and the last surviving orbit only. Thus it may easily be generalized to other systems [10, 24]. As the method only needs local information for a few prominent orbits, the approach establishes a more efficient method to calculate the topological entropy than provided by periodic orbit theory and by formal scattering methods. The latter methods need global information on the structure of the invariant set: Periodic orbit theory is based on detailed knowledge of the grammatical rules of the symbolic dynamics of the system [25], and the scattering method needs detailed information on the hierarchical structure of the time delay function of the system [19]. On the other hand, these approaches provide much more information, as they allow to calculate the full multifractal spectra.

Acknowledgements

This paper was presented at the forth annual meeting of ENGADYN, "Workshop on Nonlinearities, Dynamics and Fractals, Grenoble, 1993". The author would like to thank all members of ENGADYN for many stimulating discussions and the nice atmosphere during the workshop. He is indebted to Wolfgang Breymann for bringing Hénon's article to his attention and for many fruitful discussions, and also to H. Thomas and T. Tél for carefully reading this manuscript. This work was supported by the Swiss National Science Foundation.

Appendix A: Encoding the Billiard

In order to derive (1) we note that it is sufficient in the present context to restrict the attention to trajectories that stay in the scattering region $-1 \leq X \leq +1$ for a long time. We demand that the initial condition is chosen in such a way that the particle can turn for a given horizontal velocity $U\left(U \lesssim 2\frac{a}{r}\sqrt{\frac{2E}{m}}\right)$ and that it cannot cross the scattering region $X \in [-1, +1]$ in one jump $\left(U \lesssim \frac{mga}{2E}\sqrt{\frac{2E}{m}}\right)$. For $rE \gg mga^2$ almost all the energy of such a particle is given by its vertical motion at a reflection

$$E = mgY_i + \frac{m}{2}(U_i^2 + V_i^2) \approx \frac{m}{2}V_i^2 \quad \text{for} \quad rE \gg mga^2, \tag{A1}$$

where

m is the mass of the particle,
g the gravitational constant,
Y_i the distance from the X-axis at the reflection,
U_i the velocity in horizontal direction immediate before the i^{th} reflection,
V_i the velocity in vertical direction immediate before the i^{th} reflection.

The approximation holds because Y_i takes values between the minimum of the well at $X = 0$ and the maxima at $X = \pm a$. From $rE \gg mga^2$ it follows that the contribution from the potential energy

$$|mgY_i| \leq \frac{mga^2}{2r} \ll E$$

may be neglected.

In the limit considered, the time of flight T between successive reflections is constant. It is a function of the external parameter $\frac{E}{m}$, taking the value

$$T = \frac{2V_i}{g} \approx \left(\frac{8E}{mg^2}\right)^{1/2}. \tag{A2}$$

Here and in the following the approximation sign always refers to the limit $rE \gg mga^2$.

U_i does not change between successive reflections at X_{i-1} and X_i. Therefore it is given by

$$U_i = \frac{X_i - X_{i-1}}{T} \approx \left(\frac{mg^2}{8E}\right)^{1/2}(X_i - X_{i-1}). \tag{A3}$$

In addition, the change in U_i due to a reflection at X_i may be calculated from the angles θ_i^{in} and θ_i^{out} between the vertical line and the velocity vector of the particle immediately before and after reflection, respectively, because

$$U_i = (U_i^2 + V_i^2)^{1/2} \sin\theta_i^{\text{in}} \approx \left(\frac{2E}{m}\right)^{1/2} \theta_i^{\text{in}}. \quad \text{(A 4)}$$

The in-going and out-going angles are related by

$$\theta_i^{\text{out}} = -\theta_i^{\text{in}} + 2\arcsin\left(\frac{a\sigma_i - X_i}{r}\right) \approx -\theta_i^{\text{in}} - \frac{2}{r}(X_i - a\sigma_i), \quad \text{(A 5)}$$

where

$$\sigma_i = \text{sign}(X_i) \quad \text{(A 6)}$$

determines whether the particle is reflected at the left ($\sigma_i = -1$) or the right ($\sigma_i = +1$) disk. Using the fact that the incoming angle at the following reflection θ_{i+1}^{in} equals θ_i^{out} up to a change in sign, one obtains for U_{i+1}

$$U_{i+1} \approx \left(\frac{2E}{m}\right)^{1/2}\left(\theta_i^{\text{in}} + \frac{2}{r}(X_i - \sigma_i)\right) = U_i + \left(\frac{8E}{mr^2}\right)^{1/2}(X_i - a\sigma_i). \quad \text{(A 7)}$$

Inserting (A 3) into (A 7) and writing the resulting difference equation in matrix form immediately yields the map (1). In doing this we fixed the length scale by setting $a = 1$.

[1] M. Hénon, Physica **D 33,** 132 (1988).
[2] J. Vollmer, W. Breymann, and R. Schilling, Phys. Rev. B **47,** 11767 (1993).
[3] J. Vollmer and W. Breymann, Helv. Phys. Acta **66,** 91 (1993); J. Vollmer, Helv. Phys. Acta **66,** 905 (1993).
[4] J. M. Petit and M. Hénon, Icarus **6,** 536 (1986).
[5] S. Aubry, in: Physics of Defects (R. Balian, M. Kléman, and J.-P. Poivier, eds.) (North Holland, Amsterdam, 1981); S. Aubry, Physica **7D,** 240 (1983).
[6] P. Reichert and R. Schilling, Phys. Rev. **B 32,** 5731 (1985); R. Schilling, in: Nonlinear Dynamics in Solids (H. Thomas, ed.), Springer, Berlin 1992; P. Häner and R. Schilling, Europhys. Lett. **8,** 129 (1989); L. I. Manevich and G. M. Sigalov, Sov. Phys. Solid State **34,** 210 (1992).
[7] W. Breymann and C. Jung, Europhys. Lett. **25,** 509 (1994).
[8] P. Szepfalusy and T. Tél, Physica **16 D,** 252 (1985).
[9] T. Tél, Phys. Lett. A **97,** 219 (1983).
[10] J. Vollmer and W. Breymann, Europhys. Lett. **27,** 23 (1994).
[11] C. Grebogi, E. Ott, and J. A. Yorke, Phys. Rev. Lett. **48,** 1507 (1982); C. Grebogi and E. Ott, Physica **7 D,** 181 (1983); C. Grebogi, E. Ott, F. Romeiras, and J. A. Yorke, Phys. Rev. A **36,** 5365 (1987).
[12] Y.-C. Lai, C. Grebogi, R. Blümel, and I. Kan, Phys. Rev. Lett. **71,** 2212 (1993).
[13] I. M. Jánosi and T. Tél, Phys. Rev. E. **49,** 2756 (1994).
[14] F. Takens, in: Dynamical Systems and Turbulence (D. A. Rand and L.-S. Young, eds.), Springer Lect. Notes in Math. **898,** Springer-Verlag, Berlin 1980.
[15] In Appendix A and (1) we used the same notation as in [1]. Note however, that the coordinate x introduced in (5) of the present paper and (22) in Hénon's paper are different. The eigenvalues $\eta^{\pm 1}$ of the linear map are given by $\exp(\mp\phi)$ in Hénons notation. Hénon uses $a = 1$ throughout his paper.
[16] W. Breymann and J. Vollmer, J. Stat. Phys. **76,** 1439 (1994).
[17] J. Guckenheimer and Ph. Holmes, Nonlinear Oscillations, Dynamical Systems, and Bifurcations of Vector Fields, Springer Verlag, Berlin 1983.
[18] P. Grassberger, Z. Naturforsch. **43 a,** 671 (1988).
[19] T. Tél, in: Directions in Chaos, Vol. 3: Experimental Study and Characterization of Chaos (Hao Bai-Lin, ed.), World Scientific, Singapore 1990.
[20] I. Procaccia, Nature, London **333,** 618 (1988).
[21] V. I. Arnold and A. Avez, Ergodic Problems in Classical Mechanics, Benjamin, New York 1968.
[22] Z. Kovács and T. Tél, Phys. Rev. Lett. **64,** 1617 (1990); T. Tél, Phys. Rev. A **44,** 1034 (1991); Y. T. Lau, J. M. Finn and E. Ott, Phys. Rev. Lett. **66,** 978 (1991).
[23] R. W. Leven, B. Pompe, C. Wilke, and B. P. Koch, Physica **D 16,** 371 (1985); T. L. Caroll, L. M. Pecora and F. J. Rachford, Phys. Rev. **B 38,** 2938 (1988); W. L. Ditto et al., Phys. Rev. Lett. **63,** 923 (1989).
[24] W. Breymann and J. Vollmer, A Universal Scenario at the Onset of Pruning, in preparation.
[25] D. Auerbach, P. Cvitanović, J. P. Eckmann, G. H. Gunaratne, and I. Procaccia, Phys. Rev. Lett. **58,** 2387 (1987); I. Procaccia, Nature, London **333,** 618 (1988); P. Cvitanovič, G. H. Gunaratne, and I. Procaccia, Phys. Rev. A **38,** 1503 (1988); R. Artuso, E. Aurell, and P. Cvitanovič, Nonlinearity **3,** 325 and 361 (1990); B. Eckardt, in: Lecture Notes of the International School of Physics, Enrico Fermi on Quantum Chaos (1991).